

Article

The Mechanical Consequences of the Interplay of Mineral Distribution and Organic Matrix Orientation in the Claws of the Sea Slater *Ligia pallasii*

Miloš Vittori ^{1,*}, Vesna Srot ², Lidija Korat ³, Matjaž Rejec ⁴, Pavel Sedmak ⁵, Birgit Bussmann ², Felicitas Predel ², Peter A. van Aken ²  and Jasna Štrus ¹

¹ Department of Biology, Biotechnical Faculty, University of Ljubljana, SI-1000 Ljubljana, Slovenia; jasna.strus@bf.uni-lj.si

² Stuttgart Center for Electron Microscopy, Max Planck Institute for Solid State Research, Heisenbergstrasse 1, 70569 Stuttgart, Germany; v.srot@fkf.mpg.de (V.S.); b.bussmann@fkf.mpg.de (B.B.); f.predel@fkf.mpg.de (F.P.); p.vanaken@fkf.mpg.de (P.A.v.A.)

³ Slovenian National Building and Civil Engineering Institute, SI-1000 Ljubljana, Slovenia; lidija.korat@zag.si

⁴ Anton Paar d.o.o., Tbilisijska 57b, SI-1000 Ljubljana, Slovenia; matjaz.rejec@anton-paar.com

⁵ Anton Paar TriTec SA, Vernets 6, 2035 Corcelles, Switzerland; pavel.sedmak@anton-paar.com

* Correspondence: milos.vittori@bf.uni-lj.si



Citation: Vittori, M.; Srot, V.; Korat, L.; Rejec, M.; Sedmak, P.; Bussmann, B.; Predel, F.; van Aken, P.A.; Štrus, J. The Mechanical Consequences of the Interplay of Mineral Distribution and Organic Matrix Orientation in the Claws of the Sea Slater *Ligia pallasii*. *Minerals* **2021**, *11*, 1373. <https://doi.org/10.3390/min11121373>

Academic Editors: Vincent V. Barbin and Frédéric Marin

Received: 18 October 2021

Accepted: 3 December 2021

Published: 6 December 2021

Publisher's Note: MDPI stays neutral with regard to jurisdictional claims in published maps and institutional affiliations.



Copyright: © 2021 by the authors. Licensee MDPI, Basel, Switzerland. This article is an open access article distributed under the terms and conditions of the Creative Commons Attribution (CC BY) license (<https://creativecommons.org/licenses/by/4.0/>).

Abstract: Exposed regions of the arthropod exoskeleton have specialized structure and mineral composition. Their study can provide insights into the evolutionary optimization of the cuticle as a material. We determined the structural and compositional features of claws in the crustacean *Ligia pallasii* using X-ray micro-computed tomography, scanning electron microscopy (SEM), and analytical scanning transmission electron microscopy (STEM). In addition, we used nanoindentation to determine how these features fine-tune the mechanical properties of the claw cuticle. We found that the inner layer of the claw cuticle—the endocuticle—contains amorphous calcium phosphate, while the outer layer—the exocuticle—is not mineralized and contains elevated amounts of bromine. While the chitin–protein fibers in crustacean exoskeletons generally shift their orientation, they are aligned axially in the claws of *L. pallasii*. As a consequence, the claw cuticle has larger elastic modulus and hardness in the axial direction. We show that amorphous calcium phosphate mineralization and the brominated cuticle are widespread in isopod crustaceans inhabiting terrestrial habitats. We discuss how the features of the claw cuticle may aid in minimizing the likelihood of fracture. Ultimately, our study points out the features that increase the durability of thin skeletal elements.

Keywords: cuticle; biomaterial; biomineralization; arthropod; chitin; halogen; exoskeleton; calcium phosphate

1. Introduction

In arthropods, exoskeletal elements that are specialized for prey-handling, mastication, and locomotion differ in structure and composition from the general exoskeleton and are optimized by the process of natural selection in response to the functions they perform [1–3]. The cuticle of mandibles and claws of arthropods may be mineralized with calcite, apatite, amorphous calcium phosphate, or silica [2,4,5], or may not be mineralized at all but instead incorporate halogens, manganese (Mn), or zinc (Zn), resulting in fine-tuned mechanical properties that likely contribute to preventing mechanical failure [3].

The arthropod exoskeleton—their cuticle—consists of chitin fibers intimately linked with proteins [6,7]. In crustaceans, this organic matrix is generally also mineralized, incorporating calcium carbonate in the form of calcite and amorphous calcium carbonate, which may be present as a mixture with calcium phosphate [8–10]. Some regions of the cuticle may also be mineralized with calcium phosphate in the form of apatite, the mineral that also toughens vertebrate skeletons [1,2,11,12]. The generalized crustacean

cuticle consists of three layers. The first is the thin, proteinaceous epicuticle that covers the external surface and may contain hydrocarbons [13]. The two inner and generally mineralized layers are the exocuticle and the endocuticle. These two layers are generally strongly mineralized and consist of chitin–protein fibers, arranged in layers parallel to the body surface [8]. The parallel fibers in sequential layers shift their orientation helicoidally, resulting in a plywood-like periodical pattern known as the Bouligand structure [14].

The claws on the ultimate articles (dactyli) of crustacean appendages are generally subjected to particularly great mechanical stresses. In isopods, dactyli of walking legs (pereopods) bear immobile claws that isopods lean on during standing and walking [15,16] and use them for clinging and climbing. Recently, the cuticle of the claw in the terrestrial isopod *Porcellio scaber* was demonstrated to be mineralized with amorphous calcium phosphate in the claw's central region, while the external layer of the claw cuticle is not mineralized and incorporates bromine (Br). Furthermore, profound differences in the orientation of the chitin–protein fibers were found between the claw cuticle and the cuticle of the dactylus base of *P. scaber*. Most importantly, the chitin–protein fibers are aligned axially in the claw cuticle, suggesting that the claws are likely much stiffer in the axial direction [5]. This contrasts with the cuticle of the dactylus base or the dorsal body surface in *P. scaber*, in which the organic fibers are arranged in the typical Bouligand structure, likely resulting in a mechanically isotropic cuticle [5,9].

New phylogenetic findings indicate that isopods invaded terrestrial environments more than once in geological history. While species of the genus *Ligia* have traditionally been considered representatives of terrestrial isopods (Oniscidea) [17], recent molecular phylogenetic studies do not favor the placement of *Ligia* in this group. Instead, it may be more closely related to marine isopod groups [18,19]. Representatives of this genus generally inhabit rocky seashores and feed on algae [20]. Most are agile runners [20,21], although some defend themselves from predators also by clinging tightly to the substrate, a mode of defense facilitated by the broad, flattened bodies of such species [21]. The structure of the exoskeleton and its renewal in the process of molting have been studied in detail in *Ligia pallasii* and *Ligia italica* [13]. Along with this, the structure of the walking legs, their use in locomotion and their sensory physiology have been studied in *L. pallasii* and the related *Ligia oceanica* more extensively than in any other isopod [15,22,23]. Therefore, *L. pallasii* is the obvious choice for the study of claw biomechanics, as its exoskeleton, locomotion, and anatomy of appendages have been studied in great detail.

Individuals of *L. pallasii* typically exceed 3 cm in length and weigh more than a gram [24]. As *L. pallasii* runs extremely fast, which enables it to escape predators on the rocky seashores it inhabits [24], we can expect the claws on the dactyli to be exposed to exceptional loads. Despite tolerating submersion, this isopod spends almost all of its time on land [20]; therefore, it cannot rely on buoyancy in water to support its body as aquatic crustaceans do. As a result, a greater weight rests on the claws of its pereopods in comparison to aquatic isopods of similar size and the thin claws must resist fracture. The structural, compositional and mechanical properties of the claws are thus of particular interest, as they may offer new insights into how thin skeletal elements resist great mechanical forces, enabling them to perform reliably under heavy loading and strong impacts.

The purpose of this work was to identify the possible structural and mechanical adaptations of the claw cuticle in *L. pallasii* that enable the claws to withstand the great mechanical demands of this isopod's life-style. To this end, we employed electron microscopy, elemental analysis, and X-ray micro-computed tomography (micro-CT) and combined these methods with mechanical testing. This allowed us to determine the distribution and composition of mineralized cuticle in the claw, the architecture of the organic matrix of the cuticle and the effects of these characteristics on the mechanical properties of the claws.

2. Materials and Methods

2.1. Isopod Collection

Individuals of *L. pallasii* were collected by hand on rocky shores of the Pacific Ocean at Reuben Tarte Park on San Juan Island, Washington, USA. Animals were fixed in 96% ethanol. Animals were assigned to different stages of the molt cycle based on the absence or the presence and shape of sternal CaCO₃ deposits, as described in detail elsewhere [13,25].

2.2. Scanning Electron Microscopy (SEM)

For imaging with SEM, pereopods were completely dehydrated by submersion in acetone and air-dried in hexamethyldisilazane (HMDS). Dry pereopods were attached to metal holders with silver paint (SPI, West Chester, PA, USA), fractured with a disposable razor blade and sputter-coated with platinum to expose the inner layers of the claw cuticle. Fractured claws were imaged using a JSM-7500F field emission SEM (JEOL, Tokyo, Japan) at 5 kV acceleration voltage and 10 mm working distance. For cross-sectional elemental mapping with energy-dispersive X-ray spectroscopy (EDX), pereopods were dehydrated with acetone, embedded in Spurr's resin (SPI), and microtome-polished using a diamond knife (Diatome, Nidau, Switzerland) and an EM UC6 ultramicrotome (Leica, Wetzlar, Germany). Polished samples were evaporation-coated with carbon. Elemental mapping was performed at 10 kV using a DSM 982 Gemini SEM (Zeiss, Oberkochen, Germany) equipped with a Thermo Noran System 6 (Thermo Fischer Scientific, Waltham, MA, USA).

2.3. Imaging and Analytical Scanning Transmission Electron Microscopy (STEM)

For the purpose of mineral composition analysis, *L. pallasii* pereopods were dehydrated in acetone and embedded in Spurr's resin (SPI). Thin sections (250 nm) were prepared with a diamond knife (Diatome) using an EM UC6 ultramicrotome (Leica) and collected on copper grids covered with lacey carbon. High-angle annular dark-field scanning transmission electron microscopy (HAADF-STEM) imaging as well as electron diffraction experiments were performed at 60 kV using an ARM200F advanced TEM/STEM microscope (JEOL) equipped with a cold field-emission gun and a CETCOR image corrector (CEOS GmbH, Heidelberg, Germany). Electron energy loss (EELS) spectra were obtained in STEM mode using a GIF Quantum ERS post-column energy filter with dual EELS acquisition capability (Gatan Inc., Pleasanton, CA, USA) with a dispersion of 0.1 eV/channel.

2.4. X-ray Micro-Computed Tomography

For the determination of the structure of the dactylus and the distribution of mineral in three dimensions, fixed pereopods were air-dried. Tilt series of pereopods were obtained at a resolution of 0.96 μm using a μCT-400 tomograph (Xradia, Concord, CA, USA) equipped with a 20× optical objective. Dragonfly software (Object Research Systems, Montreal, QC, Canada) was used to perform density-based segmentation and 3D-reconstruction of the dactyli.

2.5. Nanoindentation Measurements

For the measurement of mechanical properties of the cuticle, fixed dactyli were air-dried, embedded in cyanoacrylate glue (Uhu, Bühl, Germany) for support and microtome-polished using a glass knife and an Ultracut S ultramicrotome (Reichert, Vienna, Austria). Claws were polished transversely and longitudinally in order to obtain values of the Young's modulus and the hardness of different regions of the claw cuticle in the axial and transverse directions. Measurements were performed at 22 °C and 30% air humidity with an UNHT³ Ultra Nanoindentation Tester (Anton Paar, Graz, Austria) using a Berkovich-type indenter. Loading was linear, with 5 mN maximum load and 5 s pause at maximum load and 30 mN/min loading and unloading rates. Results were obtained using the Oliver and Pharr method [26] with supposed sample Poisson's ratio of 0.3 for elastic modulus calculation, as previously determined for crustacean cuticle [6]. Levels of statistical significance of pairwise differences between groups were determined with the Tukey's

multiple comparisons test implementing the Copenhaver–Holland algorithm using Past software [27].

3. Results

3.1. Morphology of *Dactyli* in *L. pallasii*

Each of the 14 pereopods in *L. pallasii* (Figure 1A) ends in one outer claw (primary unguis) and one smaller inner claw (secondary unguis; Figure 1B). In adults approximately 3 cm long, the outer claw is about 500 μm long and 140 μm thick. While the inner claw is only slightly thinner, it is much shorter than the outer claw, reaching a length of about 170 μm . The claws have a characteristic, dark brown color that is quite different from the grayish cuticle of the dactylus body (Figure 1B). The outer claw has an annulus of lighter cuticle near its base (Figure 1B). While the results presented here were obtained from the outer claw, the inner claw has nearly identical ultrastructure and composition (Supplementary Material).

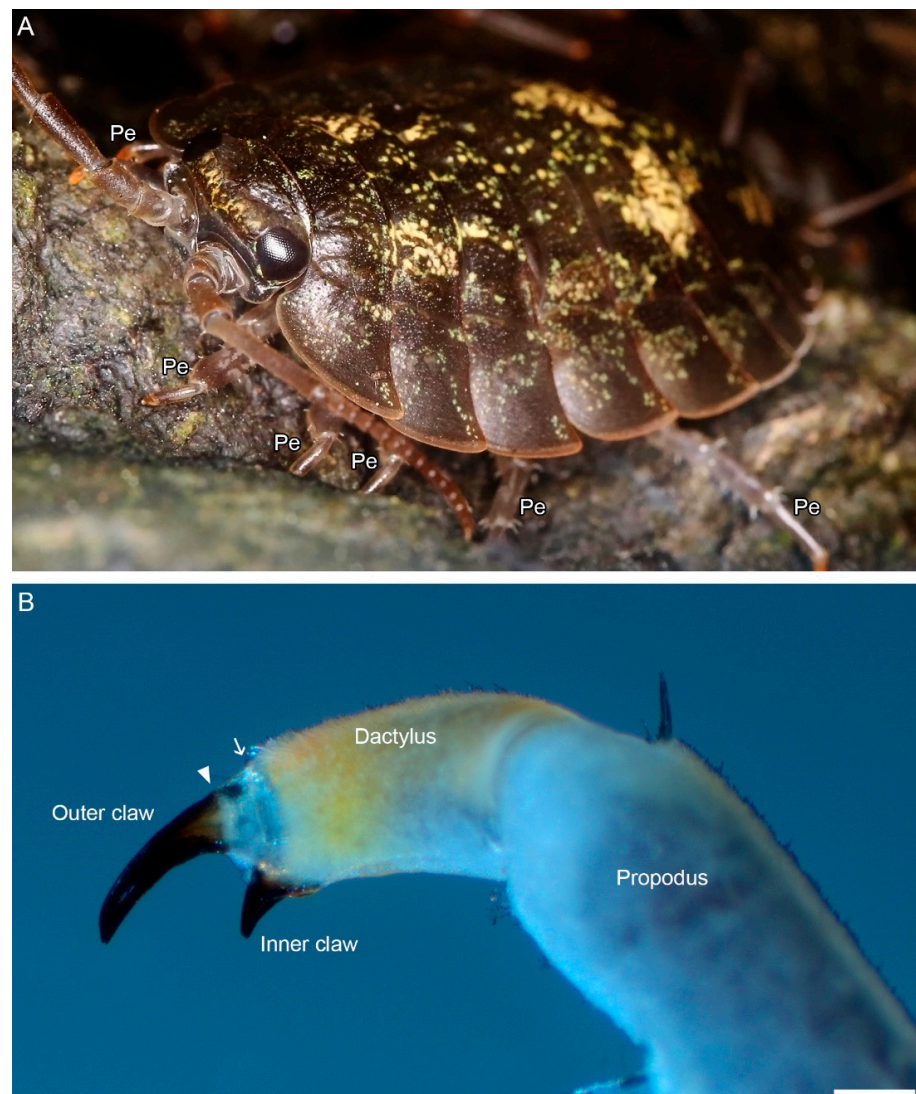


Figure 1. The isopod, *Ligia pallasii* and the distal segments of its pereopod: (A) Photograph of an adult *L. pallasii* male clinging to a rock with its pereopods (Pe). (B) Light micrograph of the distal end of a pereopod, showing the outer claw and the inner claw on the dactylus. The arrowhead points to the annulus of the outer claw and the arrow to the transition between the claw and the body of the dactylus. Scale bar: 200 μm .

3.2. Distribution of Mineral in the Dactylus Cuticle

Backscatter electron (BSE) imaging of polished, resin-embedded samples enabled us to visualize the scattering potential of different regions of the dactyli in cross-section. Together with EDX elemental mapping using SEM, we were able to determine the distribution of mineral components in the cuticle. These methods show that the cuticle of the dactylus body and in the inner cuticular layers of the claw have higher scattering potential (Figure 2). These regions also have elevated concentrations of calcium (Ca), demonstrating that these are the mineralized regions of the dactylus (Figure 3). In the cuticle of the dactylus body, the concentration of phosphorus (P) is relatively low and it is distributed predominantly in the inner layers of the cuticle, corresponding to the inner parts of the endocuticle (Figure 3). This distribution of P resembles that observed in isopod dorsal plates (tergites), in which small amounts of calcium phosphate in the inner endocuticle likely stabilize the amorphous calcium carbonate present in this layer [9]. The more distal layers of the dactylus body cuticle, on the other hand, have very low amounts of P (Figure 3). At the bases of both claws, a small segment of the cuticle has lower scattering potential and very low amounts of calcium, demonstrating that it is not mineralized (Figures 3 and 4). In the claws, the concentration of both calcium (Ca) and P are high in the inner layers of the cuticle, whereas the relatively thick outer layers have lower scattering potential and do not contain elevated amounts of either of these elements. Instead, these non-mineralized outer layers contain elevated amounts of Br (Figure 3). In the outer claw, the transition from the mineralized to the brominated outer layers of the cuticle occurs in the region of the annulus (Figure 3). As we will show, the mineralized inner layer of the claw corresponds to the endocuticle and the outer layer—mineralized at the base of the claw and brominated distally—is the exocuticle. Some mineral is, nevertheless, present in the inner layers of the exocuticle of the claw as well (Figure 2).



Figure 2. Backscattered electron image of a polished outer claw in longitudinal section. The mineralized exocuticle (ExC) at the base of the claw becomes non-mineralized (ExN) in the region of the annulus (arrowhead). Nevertheless, some mineral (asterisk) is present in the inner layers of the exocuticle distally in the claw as well. The endocuticle (En) is mineralized throughout the claw. A thin epicuticle (Ep) covers the surface. Scale bar: 20 μm .

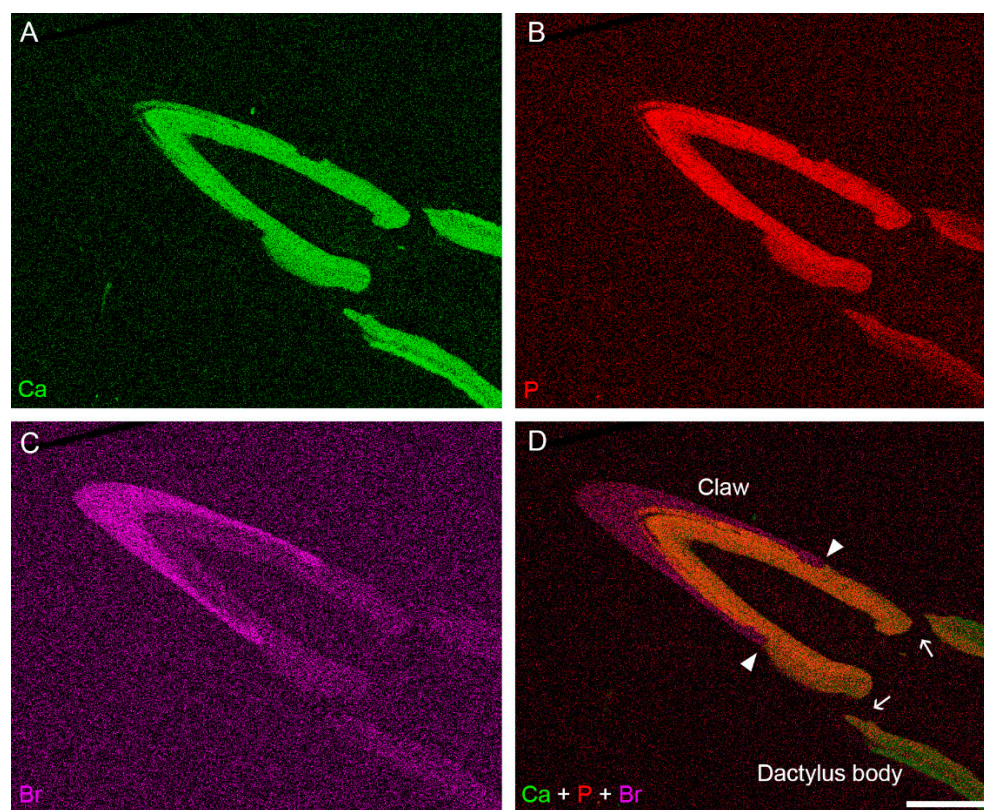


Figure 3. Elemental maps of calcium (A), phosphorus (B), and bromine (C) in the dactylus in longitudinal section, obtained with energy-dispersive X-ray spectroscopy (EDX), and an overlay elemental map showing the distribution of these three elements (D). While calcium (Ca) is present in large amounts throughout the cuticle of the dactylus body, it is only present in the inner layers of the claw cuticle. Elevated concentrations of bromine (Br) are present in the outer layer of the claw cuticle. The distribution of phosphorus (P) overlaps with that of Ca in the claw, whereas in the cuticle of the dactylus base, elevated amounts of P are only present in the innermost parts of the cuticle. A region of cuticle with lowered amounts of Ca and P is present at the base of the claw (arrows). Arrowheads show the position of the annulus on the claw. Scale bar: 50 μm .

The results of EDX elemental mapping allowed us to determine appropriate density-based segmentation thresholds of image series obtained with micro-CT to visualize the three-dimensional distribution of the mineralized regions of the exoskeleton in the dactylus (Figure 4). In this way, we were able to determine that the mineral is present throughout the cuticle of the dactylus, but only in the inner regions of the claws (Figure 4). The tips and the outer sheaths of both claws are devoid of the mineral; these are the brominated layers of the claw cuticle (Figures 3 and 4). As seen in cross-section, some regions of the dactylus cuticle lack mineral; these are the areas where each claw is joined to the dactylus, and a furrow running longitudinally on the ventral side of the dactylus, from the inner claw to about half the dactylus length (Figure 4). In this way, the claws link to the rest of the dactylus by flexible, non-mineralized cuticular regions, even though there are no genuine joints between the claws and the dactylus and no muscles are present that would allow their active movement. (See Figure 7 in the work of Hessler [15] for a detailed description of pereopod musculature in *L. pallasii*.)

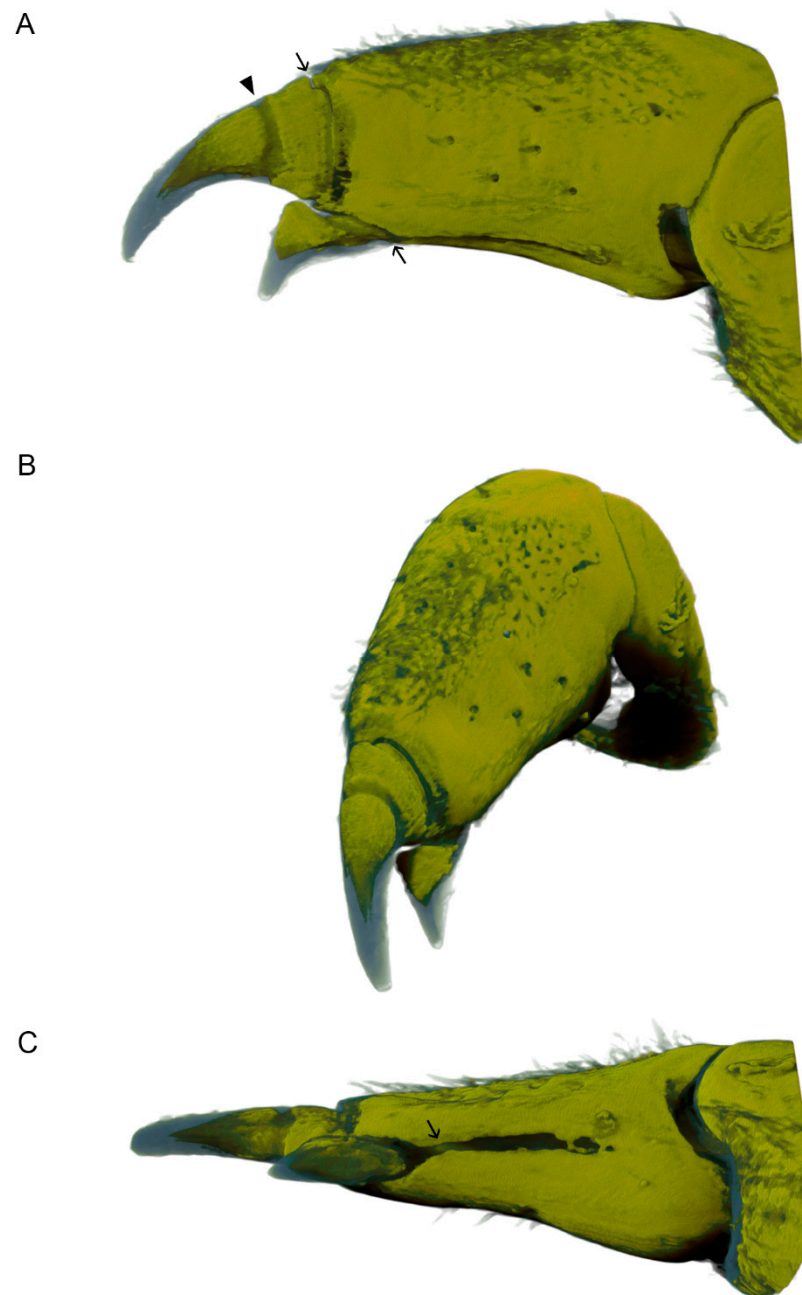


Figure 4. The three-dimensional distribution of the mineralized cuticle in the dactylus, obtained with X-ray micro-computed tomography. Mineralized cuticle is shown in light green and the non-mineralized cuticle in translucent blue. Regions of the cuticle at the bases of both claws and along a furrow on the ventral side of the dactylus are not mineralized (arrows). The exocuticle of the outer claw is not mineralized in the annulus (arrowhead), but its inner layers are mineralized again distally to this region. In both claws, the non-mineralized cuticular layer thickens towards the tip as the mineralized portion thins. (A) Posterior view. (B) lateral view. (C) Ventral view.

3.3. Ultrastructure and Mineral Composition of the Claw Cuticle

As demonstrated by SEM, the cuticle of the dactylus body follows the general crustacean pattern and is similar in structure to the cuticle of tergites in *L. pallasii* [13]. The outermost epicuticle is approximately 2 μm thick and forms scales that cover the surface of the dactylus body (Figure 5). The underlying exocuticle and endocuticle are 5 μm and 15 μm thick, respectively (Figure 5). In these two layers, chitin–protein fibers shift their orientation periodically, resulting in the characteristic Bouligand structure (Figure 5B).

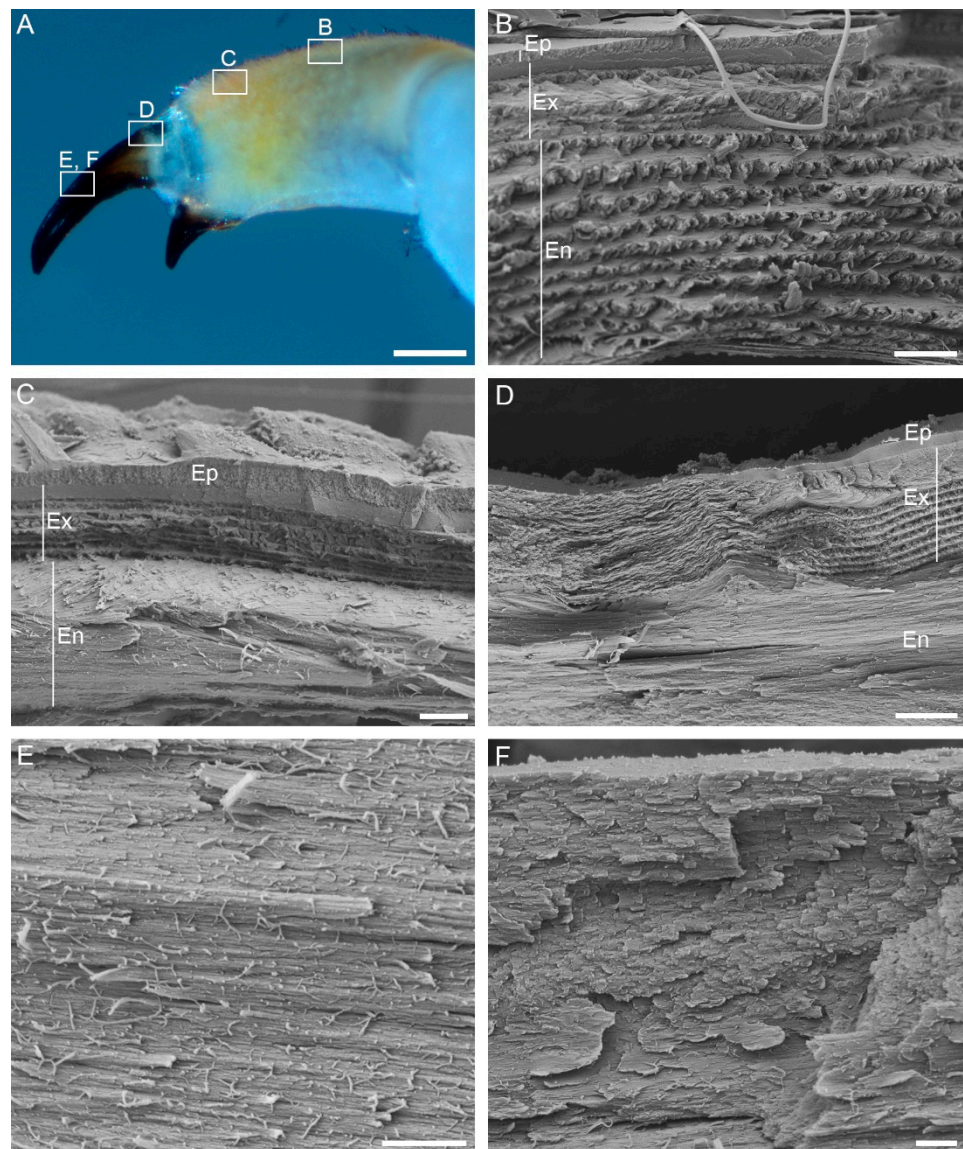


Figure 5. Organization of the cuticle in different regions of the dactylus: (A) An overview image showing the regions of the dactylus depicted in images (B–F). (B) Cuticle at the base of the dactylus resembles that of other regions of the exoskeleton, with a thin, homogeneous epicuticle (Ep), an exocuticle (Ex) with a smooth distal layer, and an endocuticle (En). The chitin–protein fibers of the exocuticle and the endocuticle are arranged in the Bouligand structure. (C) Distally in the dactylus body, the fibers of the endocuticle align in the axial direction, while the exocuticle maintains the Bouligand structure. (D) In the region of the annulus of the outer claw, the fibers of the exocuticle align as well and the epicuticle becomes thinner. (E) The endocuticle in the claw consists of axially aligned organic and mineral components. (F) The matrix components of the brominated claw exocuticle are aligned in the axial direction as well. The tip of the claw is to the left in all images. Scale bars: (A): 200 μm ; (B–D): 5 μm ; (E) and (F): 1 μm .

In the distal region of the dactylus body, the chitin–protein fibers of the endocuticle align axially and the Bouligand structure is limited to the exocuticle in this region (Figure 5C). This organization of fibers in the endocuticle continues into the claws, in which the fibers of the exocuticle align in the axial direction as well. In the outer claw, this change in organization of the exocuticle occurs in the region of the annulus, where the mineralized exocuticle of the dactylus body transitions to the brominated exocuticle of the claw (Figure 5D). While the

exocuticle thickens considerably in the claw cuticle, the epicuticle becomes thinner in distal parts of the claws (Figure 5D).

HAADF-STEM allowed us to determine the organization of organic and mineral components of the cuticle at the nanometer scale. Mineral components of the cuticle are visible as areas of high scattering potential in HAADF-STEM images. The chitin–protein fibers—visible as darker filaments in the mineralized matrix of the cuticle—shift their orientation in accordance with the Bouligand structure in the base of the claw (Figure 6) and are aligned in the distal regions of the claw cuticle (Figure 6). The axial orientation of fibers is also distinguishable in the brominated exocuticle of the claw, which displays oblique striations in longitudinal section (Figure 6D).

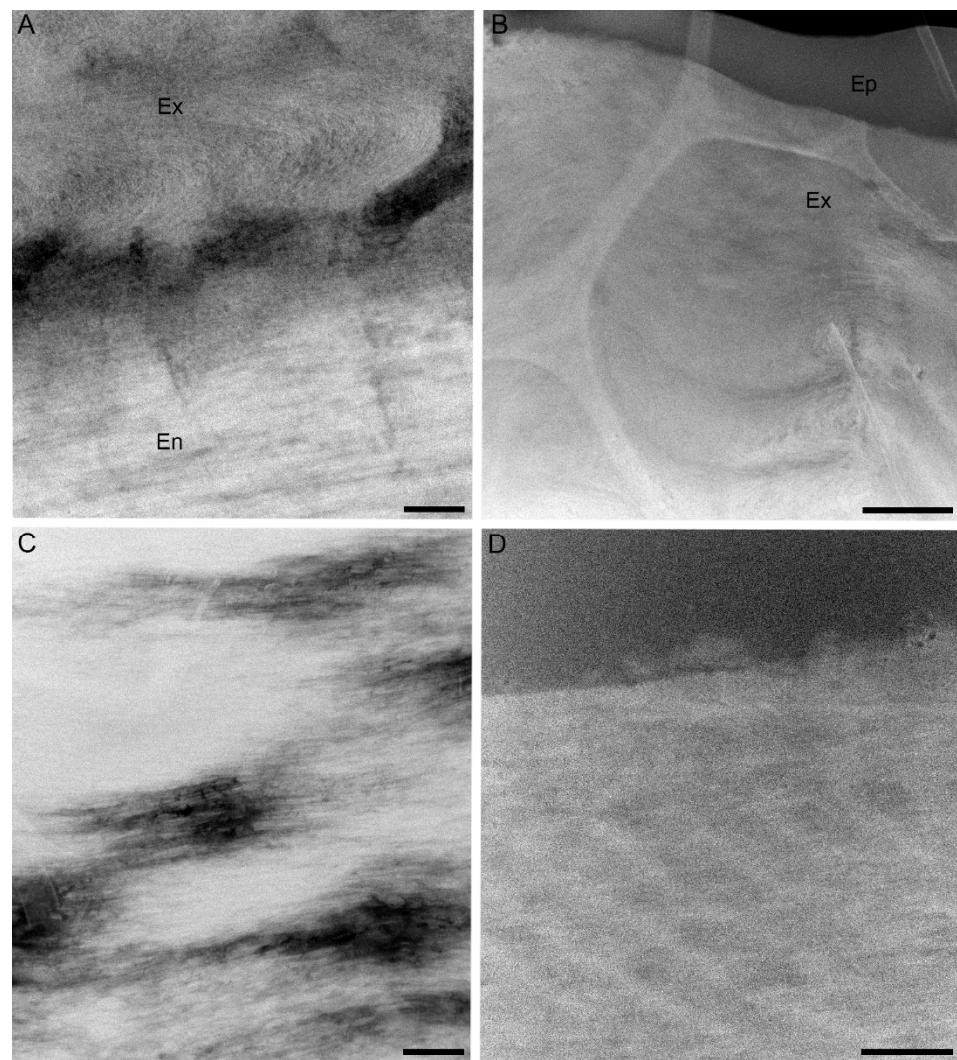


Figure 6. Ultrastructure of the dactylus cuticle in longitudinal section: (A) High-angle annular dark-field (HAADF) image of the cuticle at the base of the outer claw showing how the chitin–protein fibers of the cuticle follow the Bouligand structure in the exocuticle and are aligned axially in the endocuticle. (B) The transition from the Bouligand structure to aligned fibers and loss of mineral in the exocuticle of the annulus. (C) Aligned fibers in the claw endocuticle. (D) The brominated claw exocuticle with oblique striations with higher scattering potential. The tip of the claw is positioned towards the left in all images. Scale bars: (A): 100 nm; (B): 1 μ m; (C) and (D): 500 nm.

As determined with EDX, energy-loss near-edge structures (ELNES), and selected area electron diffraction (SAED) investigations, the dominant mineral in the claw endocuticle is amorphous calcium phosphate (ACP; Figure 7). EDX spectra show a high concentration of

P in addition to Ca, characteristic of calcium phosphates (Figure 7A). Elevated amounts of magnesium (Mg) are also demonstrated (Figure 7A). The low-loss EELS and the Ca-L_{2,3} energy loss near-edge structure (ELNES) of the mineral in the claw correspond to the fingerprint spectra of calcium phosphates [28] (Figure 7C,D), while the characteristic O-K ELNES matches that of ACP, in which the main peak of the O-K edge shows asymmetrical shape [29,30] (Figure 7E). Selected area electron diffraction (SAED) confirms the amorphous nature of the mineral in the claw endocuticle, as the mineral particles produce a diffuse diffraction pattern (Figure 7F).

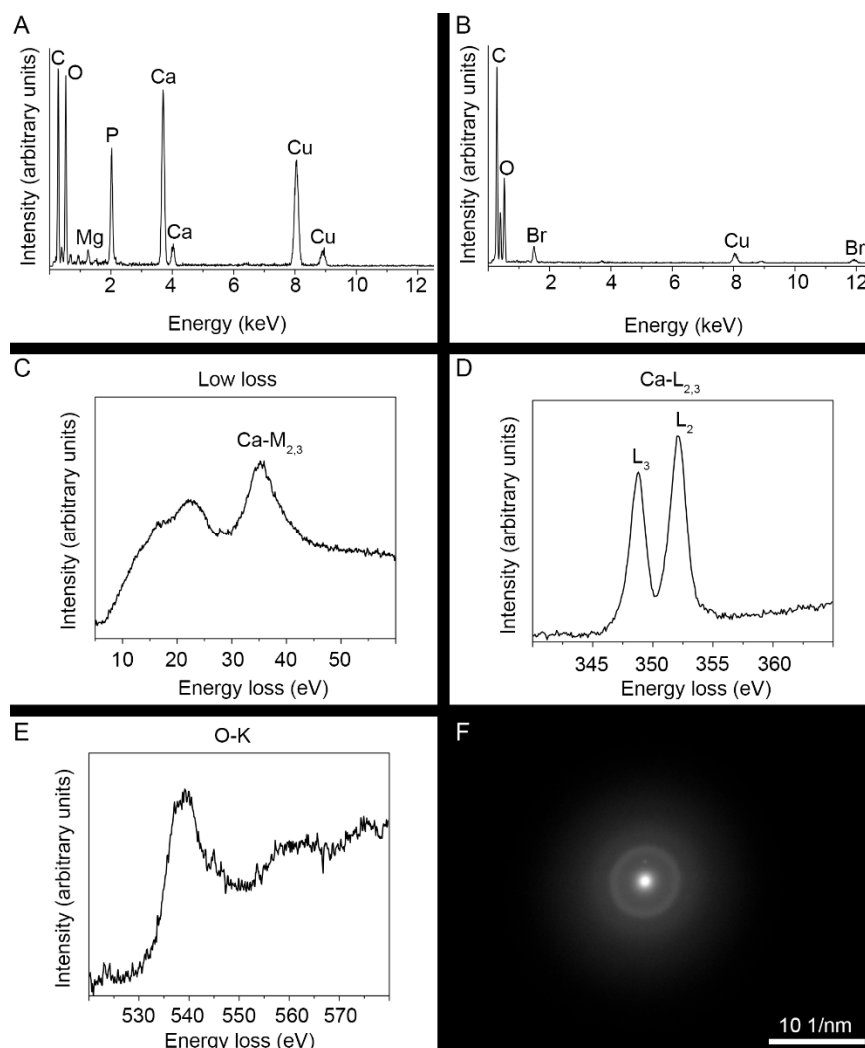


Figure 7. Mineral composition of the claw cuticle: (A) EDX spectrum of the claw endocuticle, showing the high relative concentrations of Ca and P and elevated amounts of magnesium (Mg). The copper (Cu) peak originates from the copper support grid. (B) EDX spectrum of the non-mineralized claw exocuticle, showing the presence of Br. (C) Low-loss electron energy-loss spectrum (EELS) of the mineral in the claw endocuticle. (D) The Ca-L_{2,3} energy-loss near-edge structure (ELNES) of the mineral, matching the signature spectrum of calcium phosphate. (E) The O-K ELNES of the mineral in the claw endocuticle, matching that of amorphous calcium phosphate. (F) A selected area electron diffraction pattern obtained from the mineral in the claw endocuticle, demonstrating that the mineral is amorphous.

3.4. Mechanical Properties of the Claw Cuticle

Nanoindentation measurements performed on the outer claws of *L. pallasii* show that the elastic modulus of the mineralized endocuticle as well as in the non-mineralized

exocuticle are larger in the axial than in the transverse direction (Figure 8 and Table 1). The Young's modulus of the mineralized endocuticle was approximately 26 GPa in the axial direction and 18 GPa in the transverse direction, while the Young's modulus of the non-mineralized exocuticle was approximately 15 GPa in the axial direction and approximately 6.5 GPa in the transverse direction (Figure 8 and Table 1). All modulus of elasticity values differed significantly between each other ($p < 0.001$), except for the exocuticle in the axial direction and the endocuticle in the transverse direction ($p = 0.41$). This demonstrates that the structural anisotropy of the claw cuticle translates to a mechanical anisotropy, with the claw cuticle being stiffer in the axial direction. The measured hardness of the mineralized endocuticle is approximately 1.5 GPa and 0.8 GPa in the axial and the perpendicular direction, respectively, and 0.7 GPa and 0.3 GPa in the axial and perpendicular direction in the case of the non-mineralized exocuticle (Figure 8 and Table 1). The hardness of the exocuticle in the axial direction and the hardness of the endocuticle in the transverse direction do not differ significantly ($p = 0.90$). Differences between all other hardness values are significant ($p = 0.02$ for the comparison between the endocuticle and the exocuticle in the transverse direction and $p < 0.001$ for other comparisons). The modulus of elasticity and hardness of the mineralized and the brominated cuticle of the claw are thus greater in the axial direction.

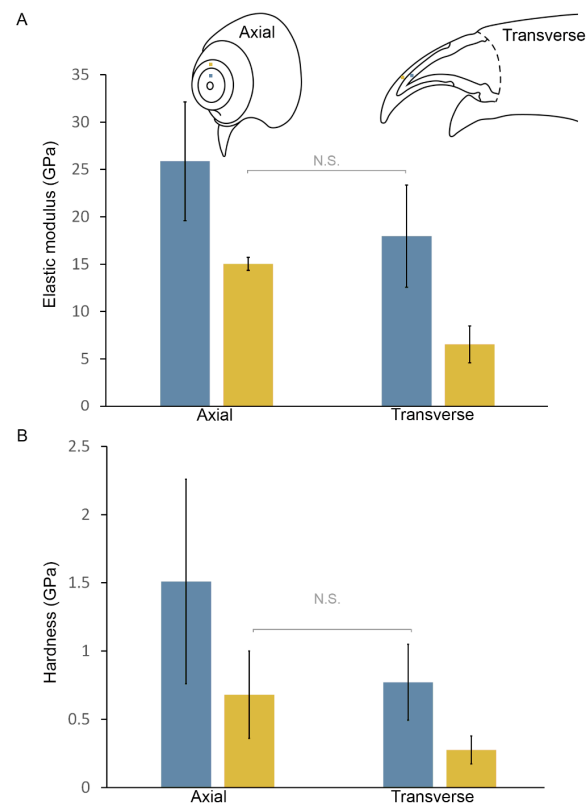


Figure 8. Mechanical properties of the claw cuticle: (A) Mean values of elastic modulus in the axial (left pair of columns) and transverse (right pair of columns) direction for the mineralized (blue) and brominated (yellow) claw cuticle. Diagrams at the top of the image show the approximate measurement positions. Differences between all values are significant ($p < 0.001$), except between the axial modulus of elasticity of the brominated cuticle and the transverse modulus of elasticity of the mineralized cuticle (N.S.). (B) Mean values of hardness in the axial (left pair of columns) and transverse (right pair of columns) direction for the mineralized (blue) and brominated (yellow) claw cuticle. Differences are statistically significant between all groups, except between the hardness of the brominated cuticle in the axial direction and the hardness of the mineralized cuticle in the transverse direction (N.S.). Error bars represent standard deviation.

Table 1. Elastic modulus and hardness of the mineralized and brominated claw cuticle in the axial and in the transverse directions. Mean values with standard deviation are presented.

| | Mineralized Cuticle, Axial Direction | Mineralized Cuticle, Transverse Direction | Brominated Cuticle, Axial Direction | Brominated Cuticle, Transverse Direction |
|--|---|--|--|---|
| Elastic modulus (GPa) ± s. d. | 25.9 ± 6.3 | 17.9 ± 5.4 | 15.0 ± 0.7 | 6.5 ± 1.9 |
| Hardness (GPa) ± s. d. | 1.5 ± 0.7 | 0.8 ± 0.3 | 0.7 ± 0.3 | 0.3 ± 0.1 |
| Number of individuals/number of measurements | 1/8 | 2/18 | 1/9 | 2/19 |

4. Discussion

The cuticle of *L. pallasii* claws is structurally and mechanically anisotropic. The central endocuticle is mineralized with ACP, whereas the external exocuticle is largely not mineralized but brominated.

It has previously been demonstrated that ACP is present in the claws of the terrestrial isopod *P. scaber*, which have a similar mineral composition and distribution of mineralized and non-mineralized cuticular layers [5]. Mineralization with ACP was reported also from the central region of the pars incisiva of the mandible in *P. scaber* [31] and in the large setae on the pereopods in the same species [30]. In contrast to decapods and stomatopods, in which calcium phosphate is found in the form of apatite, particularly in the mandibles and raptorial appendages [1,12], isopods apparently rely predominantly on ACP in the mineralized cuticle of exposed skeletal elements. The mineral in the claws of *L. pallasii* shows elevated Mg content. It has been demonstrated that Mg stabilizes ACP [32], which may be its function in the claws of *L. pallasii*.

The dactyli of isopods generally have two claws: the large outer claw, or primary unguis, and the smaller inner claw, or secondary unguis [17,33]. However, it has been questioned whether the inner claws in *Ligia* are homologous with the inner claws of other isopods with a terrestrial lifestyle, which are morphologically considerably different [17]. Our results show that the inner claw in *Ligia* is similar to the outer claw in all structural respects (see Supplementary Material). While the fine structure of the inner claws of Oniscidea has not been studied in detail to our knowledge, we hope that our results may aid in clarifying this issue in the future, especially considering the likely phylogenetic position of *Ligia* outside of Oniscidea [18].

As demonstrated in studies dealing with their gait, isopods—including studied species of *Ligia*—are supported by their claws when they walk [15,16,23]. Other uses of the claws include clinging to the substrate and climbing. Regardless of their use, the claws are loaded predictably at their tips and the forces acting on the claw are directed axially [5]. The orientation of organic fibers is exclusively axial in the distal cuticle of the claw. This orientation is reflected in the structuring of the mineral phase in the cuticle, as mineral is either deposited along the fibers or fills the spaces between them, which are also elongated in the axial direction. This results in an increase in hardness and toughness of the cuticle in the axial direction. The orientation of fibrous components in the claw cuticle thus results in a mechanically anisotropic structure, reinforced in the direction in which the claw is predominantly loaded.

The structural specializations of the cuticle are not limited to the claws; the endocuticle in the distal regions of the dactylus already consists of parallel, axially oriented chitin–protein fibers and regions ventrally on the dactylus and at the bases of both claws consist of non-mineralized cuticle. These non-mineralized regions may help to damp the forces resulting from a large isopod moving on land and can thus act as shock absorbers. Alternatively, these non-mineralized regions may be the result of the mechanism by which the dactylus cuticle is deposited during each molt, necessitating its invagination during preparation for molt and expansion after molt [34].

The elastic modulus of the endocuticle in the claw of *L. pallasii* is smaller in comparison with cuticles mineralized with apatite. Examples of such cuticles are the dactylus club of the smashing limb in the stomatopod *Odontodactylus scyllarus* [12] and the inner layers of the mandible in the crayfish *Cherax quadricarinatus* [2]. In these two skeletal elements, the inner cuticular layers are mineralized with a mixture of amorphous calcium carbonate and ACP and have similar elastic moduli as the mineralized cuticle of the claw in *L. pallasii*. The values of the elastic modulus of the mineralized endocuticle in *L. pallasii* are also comparable to those measured in the pars incisiva of the mandible in *P. scaber*, which are mineralized with ACP [31]. The relatively low elastic modulus and hardness are therefore characteristic of cuticle mineralized with ACP. A likely mechanical advantage of ACP is its great fracture-resistance, despite its relatively low hardness [35].

Both the hardness and the modulus of elasticity in the axial direction are larger in the non-mineralized claw exocuticle of *L. pallasii* than in the brominated exocuticle of crab claws or in the non-mineralized regions of the mandible in *P. scaber* [31]. These parameters are comparable to those measured in nereid jaws, leaf-cutter ant mandibles, and spider fangs, all of which are reinforced with Zn [3]. Nevertheless, the strengthening in the axial direction comes with a trade-off, as these parameters are lower in the transverse direction in the claws of *L. pallasii* than in similar Br- and Zn-enriched cuticles.

Giving up mineralization and employing softer, non-mineralized and highly sclerotized cuticle may be advantageous in cases where fracture-resistance is critical. Isopods surround their mineralized endocuticle with a non-mineralized, brominated layer of cuticle in their claws, a layer that is somewhat less stiff and less hard. This makes sense in light of resisting failure in an elongated structure bearing heavy loads, such as the isopod claw. While it is established that harder and stiffer materials are generally more resistant to abrasion—explaining why vertebrate teeth and crayfish mandibles are extremely hard—less brittle cuticles may be favorable in cases when resisting chipping or fractures resulting from bending is more important [3]. Arthropods may harden exposed skeletal elements by means other than biomineralization, for instance, by incorporating halogens, zinc (Zn), and manganese (Mn) into the cuticle, where they are likely bound to proteins. Such cuticles are more homogeneous, as they do not include mineral grains. This results in them being less prone to chipping [3]. In the brominated tips of claws of the crab *Pachygrapsus crassipes*, the mineralized cuticle is indeed more resistant to abrasion than non-mineralized, brominated cuticle [36]. However, the energy of fracture is much greater for the brominated cuticle than for the mineralized cuticle in this case. Furthermore, brominated cuticle can withstand much greater deformation than mineralized cuticle and has been shown to be more resistant to impact, as demonstrated by bead-blasting, which eroded the mineralized cuticle to a much greater extent than brominated cuticle [36]. It was thus proposed that fracture resistance is the major benefit of employing non-mineralized cuticle in exposed, thin skeletal elements. Brominated cuticle is also able to damp impacts better [3,36]. As in *L. pallasii*, the brominated layer of crab claws is the exocuticle, and there are indications that bromine is bound to phenyl rings of proteins in the case of crab claws [36].

Taken together, the use of stiff and hard mineralized cuticle is likely preferable in larger skeletal elements, which are more exposed to wear than fracture, whereas non-mineralized, brominated cuticle is more functional in thin and sharp skeletal elements that are in danger of breaking [3]. The incorporation of ACP and non-mineralized, brominated cuticle in the claw of *L. pallasii* together with the structural and mechanical anisotropy and a flexible link to the dactylus body that can damp impacts should all result in great fracture resistance of the claw. Such structural and compositional features can be mimicked to improve the durability of thin machine elements that come into contact with the substrate.

Supplementary Materials: The following are available online at <https://www.mdpi.com/article/10.3390/min11121373/s1>, Figure S1: Structure and composition of the cuticle in the inner claw of *Ligia pallasii*. Figure S2: HAADF-STEM image of the non-mineralized exocuticle of the inner claw in longitudinal section. Figure S3: Energy dispersive X-ray (EDX) spectrum of the mineralized endocuticle of the inner claw. Figure S4: EDX spectrum of the non-mineralized exocuticle of the inner claw.

Author Contributions: Conceptualization, M.V. and J.Š.; methodology, M.V., M.R., V.S., B.B., F.P. and L.K.; formal analysis, M.V. and V.S.; investigation, M.V., P.S., V.S., B.B., F.P. and L.K.; resources, J.Š. and P.S.; writing—original draft preparation, M.V. and V.S.; writing—review and editing, J.Š., L.K., M.R., P.S. and P.A.v.A.; visualization, M.V.; supervision, J.Š. and P.A.v.A.; project administration, P.A.v.A.; funding acquisition, M.V., J.Š. and P.A.v.A. All authors have read and agreed to the published version of the manuscript.

Funding: This research was funded by the Slovenian Research Agency, grants P1-0184 and BI-DE/19-20-016, and the German Academic Exchange Service (DAAD), grant PPP Slowenien 57451152. This work also received funding from the European Union’s Horizon 2020 research and innovation programme under grant agreement number 823717–ESTEEM3. Some of the equipment used in the study was purchased in the project “Development of research infrastructure for the international competitiveness of the Slovenian RRI space–RI-SI-LifeWatch”. The operation is co-financed by the Republic of Slovenia, Ministry of Education, Science, and Sport and the European Union from the European Regional Development Fund. The APC was funded by the University of Ljubljana, Biotechnical Faculty.

Data Availability Statement: Data is contained within the article or Supplementary Material.

Acknowledgments: The authors would like to thank the company Anton Paar for enabling the mechanical testing and Rok Kostanjšek for access to software enabling the 3D visualization of micro-CT scans. Andrej Blejec participated in animal collection and provided the photograph used in Figure 1A. This work was supported by the infrastructural center “Microscopy of biological samples” at the Biotechnical faculty, University of Ljubljana.

Conflicts of Interest: The authors declare no conflict of interest. The funders had no role in the design of the study; in the collection, analyses, or interpretation of data; in the writing of the manuscript, or in the decision to publish the results.

References

1. Amini, S.; Masic, A.; Bertinetti, L.; Teguh, J.S.; Herrin, J.S.; Zhu, X.; Su, H.; Miserez, A. Textured fluorapatite bonded to calcium sulphate strengthen stomatopod raptorial appendages. *Nat. Commun.* **2014**, *5*, 3187. [[CrossRef](#)]
2. Bentov, S.; Zaslansky, P.; Al-Sawalmih, A.; Masic, A.; Fratzl, P.; Sagi, A.; Berman, A.; Aichmayer, B. Enamel-like apatite crown covering amorphous mineral in a crayfish mandible. *Nat. Commun.* **2012**, *3*, 839. [[CrossRef](#)] [[PubMed](#)]
3. Schofield, R.M.S.; Bailey, J.; Coon, J.J.; Devaraj, A.; Garrett, R.W.; Goggans, M.S.; Hebnner, M.G.; Lee, B.S.; Lee, D.; Lovern, N.; et al. The homogenous alternative to biomineralization: Zn- and Mn-rich materials enable sharp organismal “tools” that reduce force requirements. *Sci. Rep.* **2021**, *11*, 17481. [[CrossRef](#)] [[PubMed](#)]
4. Miller, C.B.; Nelson, D.M.; Weiss, C.; Soeldner, A.H. Morphogenesis of opal teeth in calanoid copepods. *Mar. Biol.* **1990**, *106*, 91–101. [[CrossRef](#)]
5. Vittori, M.; Srot, V.; Žagar, K.; Busmann, B.; van Aken, P.A.; Čeh, M.; Štrus, J. Axially aligned organic fibers and amorphous calcium phosphate form the claws of a terrestrial isopod (Crustacea). *J. Struct. Biol.* **2016**, *195*, 227–237. [[CrossRef](#)]
6. Nikolov, S.; Petrov, M.; Lymperakis, L.; Friák, M.; Sachs, C.; Fabritius, H.O.; Raabe, D.; Neugebauer, J. Revealing the design principles of high-performance biological composites using ab initio and multiscale simulations: The example of lobster cuticle. *Adv. Mater.* **2010**, *22*, 519–526. [[CrossRef](#)]
7. Roer, R.; Abehsera, S.; Sagi, A. Exoskeletons across the Pancrustacea: Comparative morphology, physiology, biochemistry and genetics. *Integr. Comp. Biol.* **2015**, *55*, 771–791. [[CrossRef](#)] [[PubMed](#)]
8. Dillaman, R.; Roer, R.; Shafer, T.; Modla, S. The Crustacean Integument: Structure and Function. In *The Natural History of the Crustacea. Functional Morphology and Diversity*; Watling, L., Thiel, M., Eds.; Oxford University Press: Oxford, UK, 2013; Volume 1, pp. 140–166.
9. Hild, S.; Marti, O.; Ziegler, A. Spatial distribution of calcite and amorphous calcium carbonate in the cuticle of the terrestrial crustaceans *Porcellio scaber* and *Armadillidium vulgare*. *J. Struct. Biol.* **2008**, *163*, 100–108. [[CrossRef](#)]
10. Neues, F.; Ziegler, A.; Epple, M. The composition of the mineralized cuticle in marine and terrestrial isopods: A comparative study. *CrystEngComm* **2007**, *9*, 1245–1251. [[CrossRef](#)]
11. Currey, J.D.; Nash, A.; Bonfield, W. Calcified cuticle in the stomatopod smashing limb. *J. Mater. Sci.* **1982**, *17*, 1939–1944. [[CrossRef](#)]
12. Weaver, J.C.; Milliron, G.W.; Miserez, A.; Evans-Lutterodt, K.; Herrera, S.; Gallana, I.; Mershon, W.J.; Swanson, B.; Zavattieri, P.; DiMasi, E.; et al. The stomatopod dactylus club: A formidable damage-tolerant biological hammer. *Science* **2012**, *336*, 1275–1280. [[CrossRef](#)]
13. Štrus, J.; Tušek-Žnidarič, M.; Repnik, U.; Blejec, A.; Summers, A. Microscopy of crustacean cuticle: Formation of a flexible extracellular matrix in moulting sea slaters *Ligia pallasii*. *J. Mar. Biol. Assoc. UK* **2018**, *99*, 857–865. [[CrossRef](#)]

14. Bouligand, Y. Twisted fibrous arrangements in biological materials and cholesteric mesophases. *Tissue Cell* **1972**, *4*, 189–217. [[CrossRef](#)]
15. Hessler, R.R. The structural morphology of walking mechanisms in eumalacostracan crustaceans. *Philos. Trans. R. Soc. Lond. B Biol. Sci.* **1982**, *296*, 245–298.
16. Vittori, M. Structure of a hinge joint with textured sliding surfaces in terrestrial isopods (Crustacea: Isopoda: Oniscidea). *Zool. Lett.* **2021**, *7*, 7. [[CrossRef](#)]
17. Schmidt, C. Phylogeny of the terrestrial Isopoda (Oniscidea): A review. *Arthropod Syst. Phylogeny* **2008**, *66*, 191–226.
18. Dimitriou, A.C.; Taiti, S.; Sfenthourakis, S. Genetic evidence against monophyly of Oniscidea implies a need to revise scenarios for the origin of terrestrial isopods. *Sci. Rep.* **2019**, *9*, 18508. [[CrossRef](#)] [[PubMed](#)]
19. Lins, L.S.; Ho, S.Y.; Lo, N. An evolutionary timescale for terrestrial isopods and a lack of molecular support for the monophyly of Oniscidea (Crustacea: Isopoda). *Org. Divers. Evol.* **2017**, *17*, 813–820. [[CrossRef](#)]
20. Carefoot, T.H.; Taylor, B.E.; Brett, K. A day in the life of an isopod: Time and energy allocations in the semiterrestrial *Ligia pallasii*. *Isr. J. Ecol. Evol.* **1998**, *44*, 463–471.
21. Schmalzfuss, H. Eco-morphological strategies in terrestrial isopods. *Symp. Zool. Soc. Lond.* **1984**, *53*, 49–63.
22. Alexander, C.G. Observations on receptor mechanisms in *Ligia oceanica* (Linn.). *Comp. Biochem. Physiol. A Physiol.* **1971**, *40*, 339–347. [[CrossRef](#)]
23. Alexander, C.G. Locomotion in the isopod crustacean, *Ligia oceanica* (Linn.). *Comp. Biochem. Physiol. A Physiol.* **1972**, *42*, 1039–1047. [[CrossRef](#)]
24. Carefoot, T.H. Studies on the growth, reproduction, and life cycle of the supralittoral isopod *Ligia pallasii*. *Mar. Biol.* **1973**, *18*, 302–311.
25. Zidar, P.; Drobne, D.; Štrus, J. Determination of moult stages of *Porcellio scaber* (Isopoda) for routine use. *Crustaceana* **1998**, *71*, 646–654.
26. Oliver, W.C.; Pharr, G.M. Measurement of hardness and elastic modulus by instrumented indentation: Advances in understanding and refinements to methodology. *J. Mater. Res.* **2004**, *19*, 3–20. [[CrossRef](#)]
27. Hammer, Ø.; Harper, D.A.; Ryan, P.D. PAST: Paleontological statistics software package for education and data analysis. *Palaeontol. Electron.* **2001**, *4*, 4.
28. Srot, V.; Bussmann, B.; Salzberger, U.; Koch, C.T.; van Aken, P.A. Linking microstructure and nanochemistry in human dental tissues. *Microsc. Microanal.* **2012**, *18*, 509–523. [[CrossRef](#)] [[PubMed](#)]
29. Srot, V.; Bussmann, B.; Salzberger, U.; Deuschle, J.; Watanabe, M.; Pokorny, B.; Jelenko Turinek, I.; Mark, A.F.; van Aken, P.A. Magnesium-assisted continuous growth of strongly iron-enriched incisors. *ACS Nano* **2017**, *11*, 239–248. [[CrossRef](#)]
30. Vittori, M.; Srot, V.; Bussmann, B.; Predel, F.; van Aken, P.A.; Štrus, J. Structural optimization and amorphous calcium phosphate mineralization in sensory setae of a terrestrial crustacean (Isopoda: Oniscidea). *Micron* **2018**, *112*, 26–34. [[CrossRef](#)]
31. Huber, J.; Fabritius, H.-O.; Griesshaber, E.; Ziegler, A. Function related adaptations of ultrastructure, mineral phase distribution and mechanical properties in the incisive cuticle of mandibles of *Porcellio scaber* Latreille, 1804. *J. Struct. Biol.* **2014**, *188*, 1–15. [[CrossRef](#)]
32. Gelli, R.; Ridi, F.; Baglioni, P. The importance of being amorphous: Calcium and magnesium phosphates in the human body. *Adv. Colloid. Interface. Sci.* **2019**, *269*, 219–235. [[CrossRef](#)] [[PubMed](#)]
33. Khalaji-Pirbalouty, V.; Wägele, J.W. Two new species of *Ligia* Fabricius, 1798 (Crustacea: Isopoda: Ligiidae) from coasts of the Persian and Aden gulfs. *Org. Divers. Evol.* **2010**, *10*, 135–145. [[CrossRef](#)]
34. Leela Vallabhan, D. Observations on the moulting phenomenon of an isopod, *Sphaeroma walkeri*. *Proc. Indian Acad. Sci.* **1979**, *88*, 257–264. [[CrossRef](#)]
35. Saber-Samandri, S.; Gross, K.A. Amorphous calcium phosphate offers improved crack resistance: A design feature from nature? *Acta Biomater.* **2011**, *7*, 4235–4241. [[CrossRef](#)] [[PubMed](#)]
36. Schofield, R.M.S.; Niedbala, J.C.; Nesson, M.H.; Tao, Y.; Shokes, J.E.; Scott, R.A.; Latimer, M.J. Br-rich tips of calcified crab claws are less hard but more fracture resistant: A comparison of biomineralized and heavy-element biomaterials. *J. Struct. Biol.* **2009**, *166*, 272–287. [[CrossRef](#)]